Bulk and surface electronic structure of MnPSe₃ revealed by photoemission and x-ray absorption spectroscopy

Masato Fujii [1], Tomoyuki Yamaguchi,[1] Takuo Ohkochi,[2,3] Chandan De [4,5]
Sang-Wook Cheong [5,6] and Takashi Mizokawa [1]

[1]*Department of Applied Physics, Waseda University, Tokyo 169-8555, Japan*
[2]*Japan Synchrotron Radiation Research Institute, Sayo, Hyogo 679-5198, Japan*
[3]*RIKEN SPring-8 Center, Sayo, Hyogo 679-5148, Japan*
[4]*Center for Artificial Low Dimensional Electronic Systems, Institute for Basic Science (IBS), Pohang 37673, Korea*
[5]*Laboratory of Pohang Emergent Materials, Pohang University of Science and Technology (POSTECH), Pohang 790-784, Korea*
[6]*Rutgers Center for Emergent Materials and Department of Physics and Astronomy, Rutgers University, Piscataway, New Jersey 08854, USA*

Bulk and surface electronic states of MnPSe₃ have been investigated by means of x-ray photoemission spectroscopy (XPS), x-ray absorption spectroscopy (XAS), and theoretical calculations. In Mn $2p$ XPS, the main peak is accompanied by a charge-transfer satellite which is commonly observed in various Mn chalcogenides. The intensity of the charge-transfer satellite is considerably reduced by oxidization of the surface. The multiplet structure of Mn $2p$ XAS indicates the high spin Mn^{2+} configuration. The cluster model analyses of the XPS and XAS spectra indicate that the Se $4p$-to-Mn $3d$ charge-transfer energy Δ is negative providing the strong p-d hybridization. The magnetic interaction between the third nearest neighboring Mn spins is enhanced by the smallness of Δ and the unique molecular orbitals of the P_2Se_6 cluster.

I. INTRODUCTION

In transition-metal oxides with integer number of d electrons per site, the d electrons tend to be localized at each site due to the strong on-site Coulomb interaction U between them [1,2]. At each site, the d electrons follow the Hund rule and form a localized spin. The localized spins at the transition-metal sites tend to be antiferromagnetically ordered at low temperatures due to the superexchange interaction between them [1,2]. The d electrons in transition-metal chalcogenides are less localized than those in oxides partly due to the reduced magnitude of U. However, there are several antiferromagnetic and insulating transition-metal chalcogenides with localized d electrons.

MnPSe₃ is known as one of the antiferromagnetic and insulating transition-metal chalcogenides. As shown in Fig. 1, MnPSe₃ has a layered crystal structure (space group No. 148, $R\bar{3}$) in which the Mn sites form a honeycomb lattice [3,4]. MnPSe₃ shows an antiferromagnetic order below 74 K [3,4] and has an optical energy gap about 2.3 eV [6,7]. Recently, MnPSe₃ has been attracting revived interest due to the emerging physical properties of exfoliated nanosheet [8–12]. More recently, the magnetic interaction between the Mn spins has been investigated by means of inelastic neutron scattering [13]. In spite of the extensive studies of optical and magnetic properties, the electronic structure of MnPSe₃ has not been scrutinized yet. In the x-ray photoemission spectroscopy (XPS) study by Gusmao *et al.* [10], the Mn $2p$ XPS spectrum has two components, one of which is assigned to the surface contamination of MnO₂. However, it is also known

that the Mn $2p$ peak of Mn chalcogenides can be accompanied by a strong charge-transfer satellite [14,15].

In order to scrutinize the electronic structure of MnPSe₃, we have performed XPS, x-ray absorption spectroscopy (XAS), and generalized gradient approximation (GGA)+U calculations on it. The present analysis shows that MnPSe₃ belongs to the negative charge-transfer energy regime in the Zaanen-Sawatzky-Allen scheme [16–21]. The negative charge-transfer energy provides exotic electronic states with ligand holes [22–26]. In addition, the third neighbor magnetic interaction in the honeycomb lattice can be enhanced due to the negative charge-transfer energy [27,28].

II. METHODS

Single crystals of MnPSe₃ were grown by chemical vapor transport method using I₂ as a transport agent. An elemental powder mixture of Mn (99.99%; Alfa Aesar), P (99.999%; Sigma-Aldrich), and Se (99.999%; Alfa Aesar) in a molar ratio of 1 : 1 : 3 was placed and sealed in an evacuated quartz tube purged with Ar. About 8 mg/cc concentration of I₂ was added as a transport agent in the 20-cm-long tube and heated in a two-zone muffle furnace. Initially, the charge side and cold side temperature was kept inverted for 2 days to reduce the nucleation at the cold side and finally the charge side was maintained at 750 °C and the cold side at 650 °C for 21 days for the growth. The furnace was cooled down to room temperature in 10 h. Thin flakes (typically 5 mm-5 mm in size) were obtained in the cold zone.

The single crystals were fractured under vacuum of the 10^{-6} Pa range for the XPS measurements. The photoelectrons excited by Mg $K\alpha$ x ray were collected by a JEOL JPS9200 analyzer. The XAS measurements were performed at BL17SU of SPring-8 [29,30] by extracting the photon energy dependence of photoemission electron microscope image intensities around the Mn $L_{2,3}$ edge [31]. The single crystals were cleaved at 300 K under a vacuum of 10^{-5} Pa. The linearly polarized soft x ray is monochromatized by varied line spacing plane gratings with resolving power larger than 10^4. A typical spot size on the sample position is approximately $30 \times 30 \ \mu m^2$.

The GGA+U calculations with $U = 4.0$ eV and $J = 0.8$ eV were performed by QUANTUM ESPRESSO 5.30 [32,33] with pseudopotentials of Mn.pbesol-spn-kjpaw_psl.0.3.1.UPF, P.pbesol-n-kjpaw_psl.1.0.0.UPF, and Se.pbe-dn-kjpaw_psl.1.0.0.UPF. The atomic positions in the tetragonal conventional unit cell were taken from the literature [3]. The cutoff energy was set to 30 Ry. We employed the k mesh of $20 \times 20 \times 20$ in the Brillouin zone for the conventional unit cell.

The XPS and XAS spectra can be analyzed by configuration interaction calculations on the MnSe$_6$ cluster model [34]. As for Mn $2p$ XPS, the initial and final states are given by linear combinations of $d^n L^{n-5}$ configurations and by those of $cd^n L^{n-5}$ configurations ($n = 5$–10), respectively. Here, L represents a hole in the Se $4p$ orbitals and c represents a Mn $2p$ core hole. The transfer integrals between the Mn $3d$ orbitals and the Se $4p$ orbitals are parametrized by the Slater-Koster parameters $(pd\sigma)$ and $(pd\pi)$ with $(pd\pi)/(pd\sigma) = -0.45$. Although this scaling of the transfer integrals is widely used, its validity would be affected by the P$_2$Se$_6$ cluster. However, Kim *et al.* [28] showed that the Ni $2p$ XPS spectrum of NiPS$_3$ is similar to that of NiGa$_2$S$_4$ in which the scaling works well [27]. Since the scaling is valid for NiPS$_3$ with the P$_2$S$_6$ cluster, it is expected to be valid for MnPSe$_3$. The adjustable parameters are the multiplet averaged charge-transfer energy Δ and the Se $4p$-Mn $3d$ transfer integral $(pd\sigma)$. The multiplet averaged $3d$-$3d$ Coulomb interaction U and $2p$-$3d$ Coulomb interaction Q are fixed to 4.0 and 5.5 eV, respectively. These are the typical values for Mn^{2+} selenides [14,15,35]. Since the energy of $cd^6 L$ is by $Q - \Delta$ lower than that of cd^5, the $cd^7 L^2$ configuration should be included in Mn $2p$ XPS. Instead, the multiplet splitting due to the core hole is neglected, and the Hund coupling in the d^n configurations is approximated by using Kanamori parameters u, u', and j with $u - u' = 2j$ [35]. In the present model, $U = u - 20j/9$ and $j = 5B/2 + C$ where B and C are Racah parameters. Please note that the effective charge-transfer energy $\Delta_{\rm eff}$ is by $\sim 7C$ larger than Δ due to the Hund stability of the high spin d^5 configuration [36].

In the calculations for Mn $2p$ XAS, the initial (final) states are given by linear combinations of d^5 and $d^6 L$ (cd^6 and $cd^7 L$). Since the energy difference between cd^6 and $cd^7 L$ is $|\Delta + U - Q|$ and is much smaller than $|\Delta - Q|$, $cd^7 L^2$ can be neglected in Mn $2p$ XAS. Instead, the multiplet splitting should be fully included. The off-diagonal Coulomb interaction terms between the $3d$ electrons are given by the Slater integrals $F^2(3d, 3d)$ and $F^4(3d, 3d)$ which can be translated into Racah parameters B and C. In the present analysis, B and C are set to 0.125 and 0.500 eV, respectively [35,37]. The off-diagonal Coulomb interaction terms between the $2p$

core hole and the $3d$ electron are expressed by the Slater integrals $F^2(2p, 3d)$, $G^1(2p, 3d)$, and $G^3(2p, 3d)$ which are respectively fixed to 6.13, 4.62, and 2.63 eV (80% of the atomic values) [38]. In the present analysis, the ligand field splitting is derived from the difference of the p-d hybridization strength between the e_g and t_{2g} levels. Also the extra ligand field splitting due to nonorthogonality between the transition-metal $3d$ and Se $4p$ orbitals is considered [14,34]. Δ and $(pd\sigma)$ are the adjustable parameters while U and Q are fixed to 4.0 and 5.5 eV, respectively. Both for the XPS and the XAS calculations, the transfer integrals are multiplied by 0.8 in the final states considering the contraction of $3d$ wave functions due to the core hole potential [34,39].

III. RESULTS AND DISCUSSION

Figure 2 shows the Mn $2p$ XPS spectra of the clean surface and of the oxidized surface for MnPSe$_3$. The single crystal of MnPSe$_3$ was cleaved under the ultrahigh vacuum in the XPS chamber and the XPS data on the clean surface were collected. After the measurement, the crystal was taken out of the XPS chamber and exposed to the air. Then the crystal was transferred to the XPS chamber again and the XPS data on the oxidized surface were collected. In the Mn $2p$ spectrum of the clean surface, the $2p_{3/2}$ main peak is accompanied by the charge-transfer satellite as commonly observed in various Mn chalcogenides [14]. When the surface was oxidized, the binding energy of the main peak became higher than that of the clean surface. In addition, the intensity of the charge-transfer satellite was suppressed. It is known that the intensity of the charge-transfer satellite is much smaller in Mn oxides such as MnO and MnO$_2$ than that in Mn chalcogenides [15]. The Mn $2p_{3/2}$ peak of the oxidized surface is located around 641.5 eV. Since the binding energy of the Mn $2p_{3/2}$ peak is about 641 eV in MnO and about 642 eV in MnO$_2$ [40], it is difficult to identify species of the Mn oxides.

In Fig. 2, the Mn $2p$ XPS spectrum is compared with the results of MnSe$_6$ cluster model calculations. The energy separation between the main and satellite peaks is sensitive to the Δ and $(pd\sigma)$ values. The $(pd\sigma)$ value can be uniquely determined for each Δ in order to reproduce the energy separation between the main and satellite peaks. Among the trials with various Δ values, the best fit is obtained for $\Delta = -2.0$ eV and $(pd\sigma) = -1.2$ eV. The intensity of the charge-transfer satellite relative to the main peak is larger in MnPSe$_3$ than those in other Mn selenides such as Zn$_{1-x}$Mn$_x$Se. In order to reproduce the intensity ratio between the charge-transfer satellite and the main peak, the charge-transfer energy Δ should be as small as -2.0 eV. Please note that the effective charge-transfer energy $\Delta_{\rm eff}$ is still positive (about 1.5 eV) due to the Hund stability of the high-spin d^5 configuration. In the Zaanen-Sawatzky-Allen scheme [16–18], MnPSe$_3$ is located near the boundary between the charge-transfer regime ($\Delta < U$) and the negative Δ regime. Insulating transition-metal compounds with negative Δ would be rare and exotic. However, transition-metal oxides with high valence have been found to have negative Δ [19–23]. In addition, Ni chalcogenides such as NiGa$_2$S$_4$ [27] and NiPS$_3$ [28] belong to the negative Δ regime.
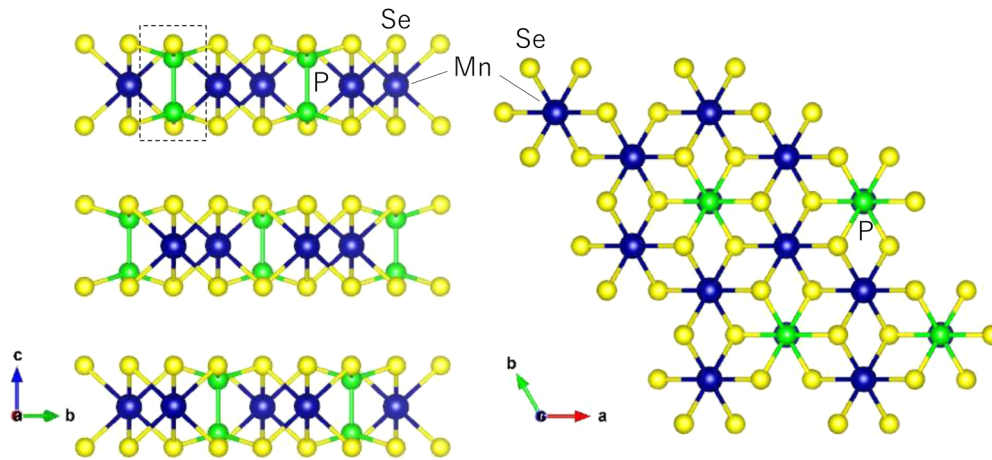
FIG. 1. Crystal structure of MnPSe$_3$ created by VESTA [5]. The left and right panels are views along the *a* axis and the *c* axis, respectively. The box drawn by dotted lines indicates the P$_2$Se$_6$ cluster.

Figure 3 shows P 2*p* and Se 3*d* XPS of the clean surface and the oxidized surface of MnPSe$_3$. The P 2*p* and Se 3*d* peaks have asymmetric line shapes due to the small spin-orbit energy splitting. As for the P 2*p* XPS spectrum of the oxidized surface, a new peak appears on the higher binding energy side which can be assigned to the oxidized P species. On the other hand, such oxidized species are not detected in the Se 3*d* XPS spectrum. These observations indicate that Mn and P are mainly oxidized during the exposure to the air. The Se 3*d* binding energy of the oxidized surface is lowered relative to that of the clean surface. Here, we speculate that the downward band bending at the clean surface of *p*-type

MnPSe$_3$ is suppressed by the oxidation causing the lowering of the Se 3*d* binding energy.

Figure 4 shows valence band XPS of the clean surface and the oxidized surface of MnPSe$_3$. In the clean surface, the valence band top reaches the Fermi level. This is consistent with the *p*-type behavior of semiconducting MnPSe$_3$. The valence band from the Fermi level to 8 eV is derived from
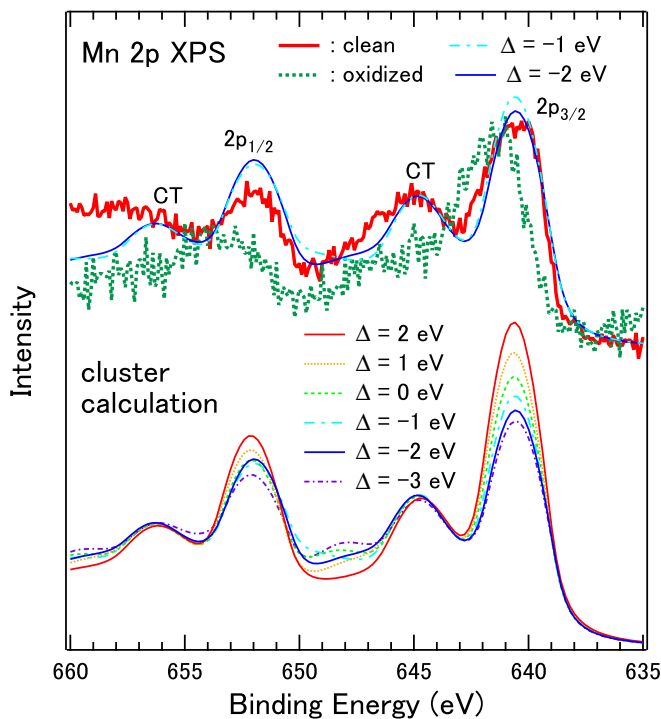

FIG. 2. Mn 2*p* XPS spectra of the clean surface (solid lines) and the oxidized surface (dotted lines). The observed spectra are compared with the results of cluster model calculations.
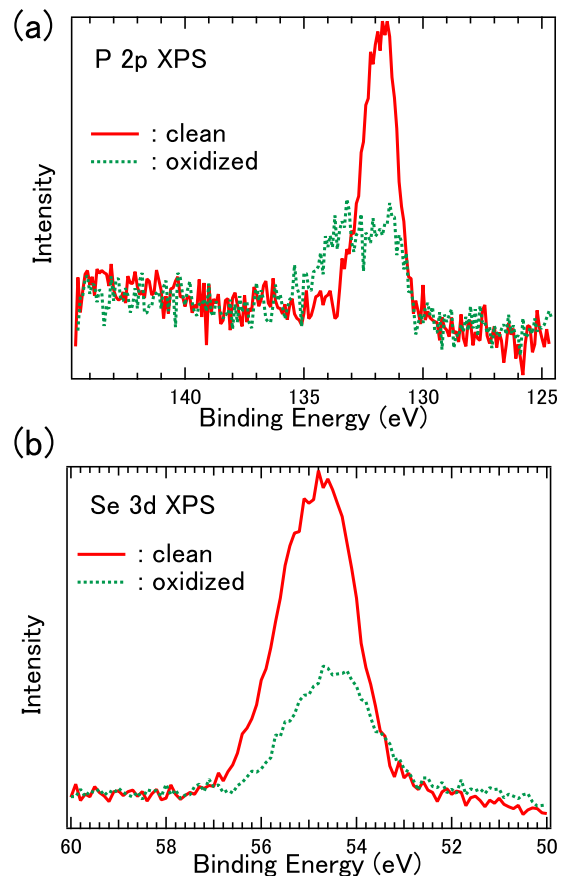

FIG. 3. (a) P 2*p* and (b) Se 3*d* XPS spectra for the clean surface (solid lines) and the oxidized surface (dotted lines).
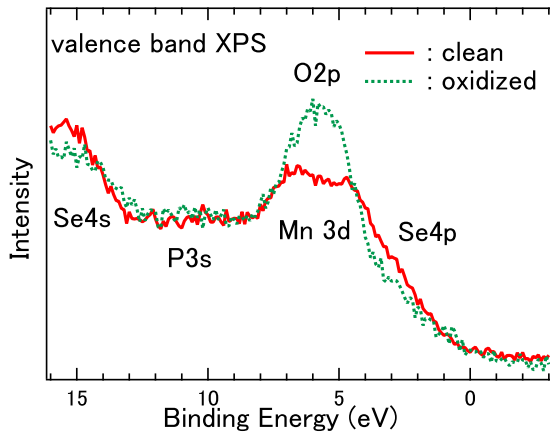
FIG. 4. Valence band XPS spectra for the clean surface (solid lines) and the oxidized surface (dotted lines).
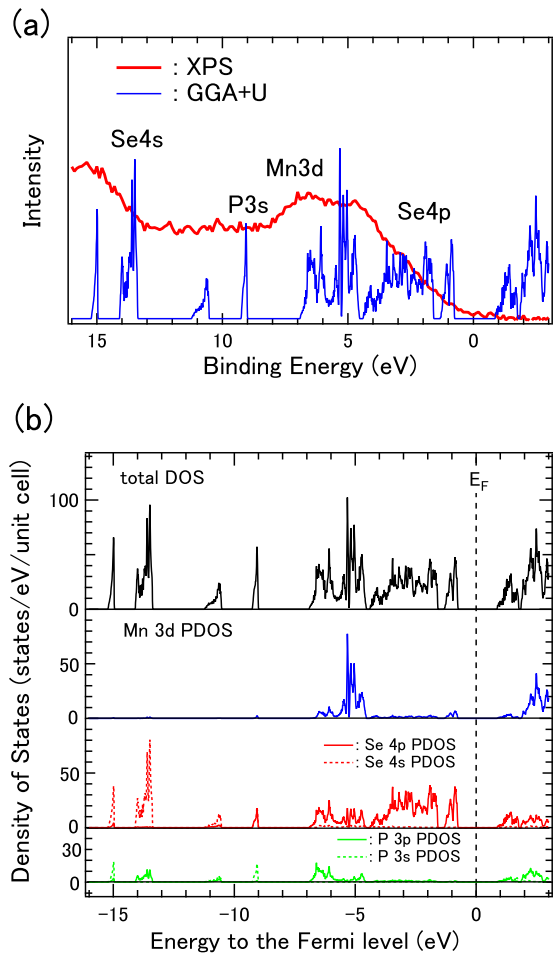

FIG. 5. (a) Comparison between the calculated density of states and the valence band XPS spectrum for the clean surface. (b) Total and partial density of states obtained by GGA+U calculations.

the Mn 3d, Se 4p, and P 3p bands. The shallow core level at 15 eV may correspond to the Se 4s and/or P 3s levels. The photoionization cross section of P 3s (0.22×10^{-2} Mb) is smaller than that of Se 4s (0.30×10^{-2} Mb) [41]. Considering the composition of P : Se = 1 : 3, the area of the P 3s peak is expected to be about 15% of that of the Se 4s peak. In the experimental result, the peak at 15 eV can be assigned to Se 4s. The P 3s peak would be located around 10 eV, which is not clearly observed. This assignment is consistent with the molecular orbital calculation for the P_2S_6 cluster by Glukhov *et al.* [42]. In the calculation, the S 3s and P 3s orbitals are mixed with the S 3p and P 3p orbitals and the bonding molecular orbitals with S 3s and P 3s characters are located around 12 and 15 eV below the reference energy level, respectively [42]. The Se 4p orbitals with a relatively large photoionization cross section (0.38×10^{-2} Mb) is mixed into the P 3s level while the P 3p orbitals with a relatively small photoionization cross section (0.88×10^{-3} Mb) is mixed with the Se 4s level [41]. In the oxidized surface, the O 2p peak evolves around 6 eV. The O 2p peak is comparable to the Mn 3d spectral weight. The Se 4p and 4s intensities are reduced by the oxidation. This is consistent with the decrease of the Se 3d intensity by the oxidation.

In Fig. 5(a), the valence band XPS spectrum is compared with the total density of states calculated by GGA+U (U=4.0 eV). Figure 5(b) shows partial density of states obtained by the GGA+U calculation. The electronic states from the Fermi level to -4 eV are dominated by Se 4p while those around -6 eV correspond to the occupied part of the Mn 3d orbitals (the lower Hubbard band). Including the Se 4s band around -15 eV, the calculated density of states is consistent with the experimental result. Interestingly, The P 3p orbitals are strongly hybridized with Mn 3d although the Mn site is octahedrally coordinated by the six Se ions and the Mn-P distance is rather large. This result indicates the strong P-Se hybridization through which the P 3p component can be mixed into the Mn 3d levels. Using the U value of 4.0 eV, the energy position of the occupied Mn 3d band agrees with the experimental result. This U value is close to that obtained by the cluster model analysis of $Cd_{1-x}Mn_xTe$ [14]. Here, it should be noted that U values for GGA+U calculations tend

to be smaller than those for cluster model analyses in various transition-metal compounds.

Figure 6 shows Mn 2p XAS for the clean surface of $MnPS_3$. The observed multiplet structure of $MnPSe_3$ is similar to the reported one for $MnPS_3$ [43]. The Mn 2p XAS spectrum is compared with the results of the configuration interaction calculations on a $MnSe_6$ cluster. Here, the 3d-3d Coulomb interaction U and the 2p-3d Coulomb interaction Q are fixed to 4.0 and 5.5 eV, respectively. The XAS spectrum is calculated for several values of the charge-transfer energy Δ and the transfer integral ($pd\sigma$). Since the multiplet structure is sensitive to the ligand field splitting which is determined by Δ and ($pd\sigma$), the Mn 2p XAS enables us to examine the values of Δ and ($pd\sigma$) determined from the Mn 2p XPS. As indicated by the vertical lines at structures A and B in Fig. 6, the energy splitting between A and B is too large with ($pd\sigma$) = -1.5 eV while it is comparable with the experimental result with ($pd\sigma$) = -1.2 eV. The intensity of structure A is too small with ($pd\sigma$) = -0.9 eV and the energy splitting between A and B is not well defined. The agreement with the experimental result is satisfactory with ($pd\sigma$) = -1.2 eV which is obtained from the Mn 2p XPS results. As for the Δ value, when ($pd\sigma$) is fixed to -1.2 eV, the energy position
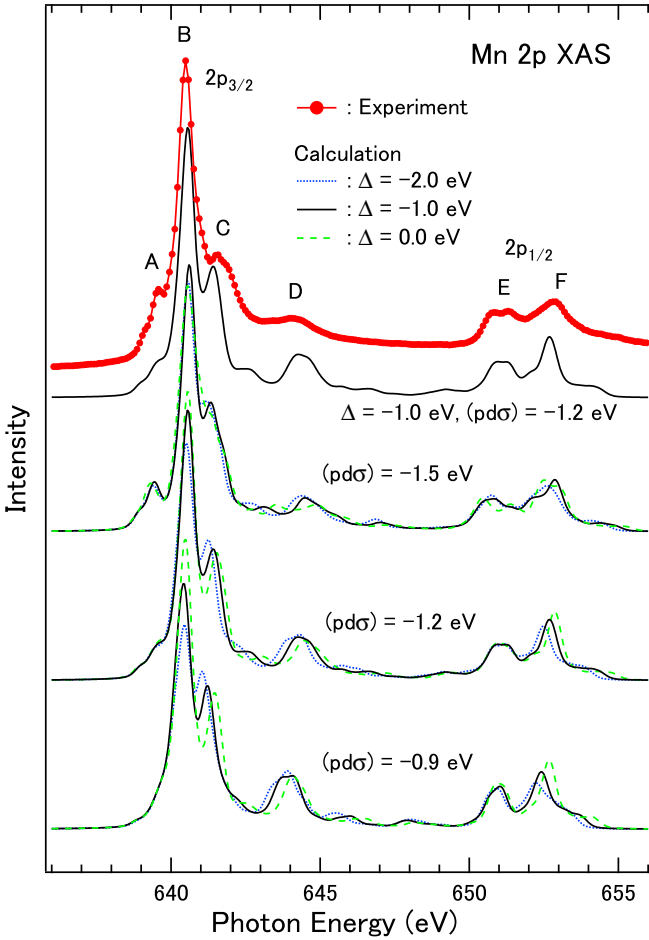
FIG. 6. Mn $2p$ XAS spectrum of MnPSe$_3$. The spectrum is compared with the cluster model calculations for $(pd\sigma) = -1.5, -1.2,$ and -0.9 eV and $\Delta = -2.0, -1.0,$ and 0.0 eV. The two vertical lines at the $2p_{3/2}$ peak indicate the energy positions of structures A and B.

of structure C around 641.5 eV is well reproduced with $\Delta = -2.0$ eV. On the other hand, the energy position of structure D around 644 eV and the spectral shapes of E and F around 651 and 653 eV are better reproduced with $\Delta = -1.0$ eV. As shown in Fig. 2, with $\Delta = -1.0$ eV, the Mn $2p$ XPS spectrum can be reproduced reasonably well although $\Delta = -2.0$ eV is certainly better. With the cluster-model analyses on the XPS and XAS results, we can safely conclude that Δ is around -1.5 ± 1.0 eV in MnPSe$_3$. These Δ values are much smaller than those reported for various Mn chalcogenides (ranging from 2.0 to 3.0 eV) [14,15]. In the ground state, the high-spin d^5 and d^6L configurations are heavily hybridized due to the negative Δ or the positive and small Δ_{eff}.

The Mn-Se hybridization is affected by the unique molecular orbitals of the P$_2$S$_6$ cluster which is not considered in the MnSe$_6$ cluster model. Although the second and third nearest neighboring Mn-Mn distances are much larger than the nearest neighboring Mn-Mn distance, the strong hybridization of Mn $3d$ with the Se and P s/p molecular orbitals provides the magnetic interactions between the second and/or third nearest neighboring Mn spins. Indeed, the neutron scattering studies

by Wildes *et al.* and Calder *et al.* revealed that the third nearest neighboring exchange interaction ($J_3 = 0.18$ or 0.19 meV) is larger than the second nearest one ($J_2 = 0.07$ or 0.03 meV) and is not negligible compared to the nearest one ($J_1 = 0.77$ or 0.45 meV) [13,44,45]. All the exchange terms are antiferromagnetic. As for the nearest neighboring bond, the direct Mn-Mn (t_{2g}-t_{2g}) transfer provides the antiferromagnetic interaction between the edge-sharing MnSe$_6$ clusters. On the other hand, the third nearest neighboring exchange interaction is derived from the Mn-P-Mn and Mn-Se-Se-Mn pathways. Takubo *et al.* showed that the magnitude of J_2 is comparable to that of J_3 in FeGa$_2$S$_4$ since both of them are derived from the Fe-S-S-Fe superexchange pathways [46]. In the case of MnPSe$_3$, the Mn-P-Mn superexchange pathway (via the P $3s$ orbital) can enhance the magnitude of J_3.

The recent spectroscopic study on NiPS$_3$ showed that the magnetic interaction between the third neighboring Ni spins can be enhanced due to the chalcogen p hole since the $d^{n+1}L$ configuration dominates the ground state of NiPS$_3$ with the negative Δ [28]. Such a mechanism was originally proposed for the triangular lattice in NiGa$_2$S$_4$ which also has the negative Δ [27]. The present work suggests that Δ is negative and Δ_{eff} is small and positive in MnPSe$_3$. The second and third neighboring magnetic interactions can be enhanced in MnPSe$_3$ similar to NiGa$_2$S$_4$ and NiPS$_3$. In addition, the P$_2$Se$_6$ cluster would enhance the third neighboring magnetic interaction. The magnetic interactions in MPQ_3 systems (M, transition metal; Q, chalcogen) should be reexamined in a systematic manner considering the molecular orbitals on the P$_2Q_6$ cluster.

IV. CONCLUSION

In conclusion, we have investigated the bulk and surface electronic states of MnPSe$_3$ by means of XPS, XAS, and GGA+U calculations. In Mn $2p$ XPS, the main peak is accompanied by a charge-transfer satellite whose intensity is reduced by oxidization of the surface. The multiplet structure of Mn $2p$ XAS indicates the high-spin Mn^{2+} configuration. The cluster model analysis indicates that the hybridization between the Mn $3d$ and Se $4p$ orbitals is substantial due to the negative Δ or the positive and small Δ_{eff}. The strong p-d hybridization is also supported by the valence band spectra and the GGA+U calculations. In addition to the negative Δ, the unique molecular orbitals of the P$_2$Se$_6$ cluster can provide the relatively strong magnetic interactions between the third nearest neighboring Mn spins.

[1] M. Imada, A. Fujimori, and Y. Tokura, Rev. Mod. Phys. **70**, 1039 (1998).

[2] D. I. Khomskii, *Transition Metal Compounds* (Cambridge University Press, Cambridge, UK, 2014).

[3] A. Wiedenmann, J. Rossat-Mignod, A. Louisy, R. Brec, and J. Rouxel, Solid State Commun. **40**, 1067 (1981).

[4] G. Le Flem, R. Brec, G. Ouvard, A. Louisy, and P. Segransan, J. Phys. Chem. Solids **43**, 455 (1982).

[5] K. Momma and F. Izumi, J. Appl. Crystallogr. **44**, 1272 (2011).

[6] R. Brec, D. M. Schleich, G. Ouvrard, A. Louisy, and J. Rouxel, Inorg. Chem. **18**, 1814 (1979).

[7] V. Grasso and L. Silipigni, J. Opt. Soc. Am. B **16**, 132 (1999).

[8] X. Li, X. Wu, and J. Yang, J. Am. Chem. Soc. **136**, 11065 (2014).

[9] B. L. Chittari, Y. Park, D. Lee, M. Han, A. H. MacDonald, E. Hwang, and J. Jung, Phys. Rev. B **94**, 184428 (2016).

[10] Rui Gusmão, Z. Sofer, and M. Pumera, Adv. Funct. Mater. **29**, 1805975 (2019).

[11] Q. Pei and W. Mi, Phys. Rev. Applied **11**, 014011 (2019).

[12] P. Liu, Z. Xu, H. Huang, J. Li, C. Feng, M. Huang, M. Zhu, Z. Wang, Z. Zhang, D. Hou, Y. Lu, and B. Xiang, J. Alloys Compd. **828**, 154432 (2020).

[13] S. Calder, A. V. Haglund, A. I. Kolesnikov, and D. Mandrus, Phys. Rev. B **103**, 024414 (2021).

[14] T. Mizokawa and A. Fujimori, Phys. Rev. B **48**, 14150 (1993).

[15] T. Mizokawa, T. Nambu, A. Fujimori, T. Fukumura, and M. Kawasaki, Phys. Rev. B **65**, 085209 (2002).

[16] J. Zaanen, G. A. Sawatzky, and J. W. Allen, Phys. Rev. Lett. **55**, 418 (1985).

[17] T. Mizokawa, A. Fujimori, H. Namatame, K. Akeyama, and N. Kosugi, Phys. Rev. B **49**, 7193 (1994).

[18] D. I. Khomskii, Lith. J. Phys. **37**, 65 (1997).

[19] T. Mizokawa, H. Namatame, A. Fujimori, K. Akeyama, H. Kondoh, H. Kuroda, and N. Kosugi, Phys. Rev. Lett. **67**, 1638 (1991).

[20] S. Nimkar, D. D. Sarma, and H. R. Krishnamurthy, Phys. Rev. B **47**, 10927 (1993).

[21] M. A. Korotin, V. I. Anisimov, D. I. Khomskii, and G. A. Sawatzky, Phys. Rev. Lett. **80**, 4305 (1998).

[22] D. Choudhury, P. Rivero, D. Meyers, X. Liu, Y. Cao, S. Middey, M. J. Whitaker, S. Barraza-Lopez, J. W. Freeland, M. Greenblatt, and J. Chakhalian, Phys. Rev. B **92**, 201108(R) (2015).

[23] V. Bisogni, S. Catalano, R. J. Green, M. Gibert, R. Scherwitzl, Y. Huang, V. N. Strocov, P. Zubko, S. Balandeh, J. Triscone, G. Sawatzky, and T. Schmitt, Nat. Commun. **7**, 13017 (2016).

[24] A. Paul, A. Mukherjee, I. Dasgupta, A. Paramekanti, and T. Saha-Dasgupta, Phys. Rev. Lett. **122**, 016404 (2019).

[25] K. Takubo, T. Mizokawa, H. Man, K. Yamamoto, Y. Zhang, Y. Hirata, H. Wadati, D. I. Khomskii, and S. Nakatsuji, Phys. Rev. B **104**, 205110 (2021).

[26] I. Leonov, Phys. Rev. B **105**, 035157 (2022).

[27] K. Takubo, T. Mizokawa, J. Y. Son, T. Nambu, S. Nakatsuji, and Y. Maeno, Phys. Rev. Lett. **99**, 037203 (2007).

[28] S. Y. Kim, T. Y. Kim, L. J. Sandilands, S. Sinn, M.-C. Lee, J. Son, S. Lee, K.-Y. Choi, W. Kim, B.-G. Park, C. Jeon, H.-D. Kim, C.-H. Park, J.-G. Park, S. J. Moon, and T. W. Noh, Phys. Rev. Lett. **120**, 136402 (2018).

[29] H. Ohashi, Y. Senba, H. Kishimoto, T. Miura, E. Ishiguro, T. Takeuchi, M. Oura, K. Shirasawa, T. Tanaka, M. Takeuchi, K. Takeshita, S. Goto, S. Takahashi, H. Aoyagi, M. Sano, Y. Furukawa, T. Ohata, T. Matsushita, Y. Ishizawa, S. Taniguchi *et al.*, *Performance of a Highly Stabilized and High-resolution Beamline BL17SU for Advanced Soft X-ray Spectroscopy at SPring-8*, AIP Conf. Proc. No. 879 (AIP, Melville, NY, 2007), p. 523.

[30] Y. Senba, H. Ohashi, H. Kishimoto, T. Miura, S. Goto, S. Shin, T. Shintake, and T. Ishikawa, *Fundamental Techniques for High Photon Energy Stability of a Modern Soft X-ray Beamline*, AIP Conf. Proc. No. 879 (AIP, Melville, NY, 2007), p. 718.

[31] T. Ohkochi, H. Osawa, A. Yamaguchi, H. Fujiwara, and M. Oura, Jpn. J. Appl. Phys. **58**, 118001 (2019).

[32] P. Giannozzi, S. Baroni, N. Bonini, M. Calandra, R. Car, C. Cavazzoni, D. Ceresoli, G. L. Chiarotti, M. Cococcioni, I. Dabo, A. Dal Corso, S. de Gironcoli, S. Fabris, G. Fratesi, R. Gebauer, U. Gerstmann, C. Gougoussis, A. Kokalj, M. Lazzeri, L. Martin-Samos *et al.*, J. Phys.: Condens. Matter **21**, 395502 (2009).

[33] P. Giannozzi, Jr., O. Andreussi, T. Brumme, O. Bunau, M. Buongiorno Nardelli, M. Calandra, R. Car, C. Cavazzoni, D. Ceresoli, M. Cococcioni, N. Colonna, I. Carnimeo, A. Dal Corso, S. de Gironcoli, P. Delugas, R. A. DiStasio, Jr., A. Ferretti, A. Floris, G. Fratesi, G. Fugallo *et al.*, J. Phys.: Condens. Matter **29**, 465901 (2017).

[34] T. Mizokawa, A. Fujimori, T. Arima, Y. Tokura, N. Mori, and J. Akimitsu, Phys. Rev. B **52**, 13865 (1995).

[35] A. E. Bocquet, T. Mizokawa, T. Saitoh, H. Namatame, and A. Fujimori, Phys. Rev. B **46**, 3771 (1992).

[36] T. Saitoh, A. E. Bocquet, T. Mizokawa, and A. Fujimori, Phys. Rev. B **52**, 7934 (1995).

[37] T. Mizokawa and A. Fujimori, Phys. Rev. B **54**, 5368 (1996).

[38] F. M. F. de Groot, J. C. Fuggle, B. T. Thole, and G. A. Sawatzky, Phys. Rev. B **42**, 5459 (1990).

[39] K. Okada and A. Kotani, J. Electron Spectrosc. Relat. Phenom. **71**, R1 (1995).

[40] V. Di Castro and G. Polzonetti, J. Electron. Spectrosc. Relat. Phenom. **48**, 117 (1989).

[41] J. J. Yeh and I. Lindau, At. Data Nucl. Data Tables **32**, 1 (1985).

[42] K. Glukhov, K. Fedyo, J. Banys, and Y. Vysochanskii, Int. J. Mol. Sci. **13**, 14356 (2012).

[43] W. Bai, Z. Hu, C. Xiao, J. Guo, Z. Li, Y. Zou, X. Liu, J. Zhao, W. Tong, W. Yan, Z. Qu, B. Ye, and Y. Xie, J. Am. Chem. Soc. **142**, 10849 (2020).

[44] A. R. Wildes, B. Roessli, B. Lebech, and K. Godfrey, J. Phys.: Condens. Matter **10**, 6417 (1998).

[45] A. Bhutani, J. L. Zuo, R. D. McAuliffe, C. R. delaCruz, and D. P. Shoemaker, Phys. Rev. Materials **4**, 034411 (2020).

[46] K. Takubo, T. Mizokawa, Y. Nambu, and S. Nakatsuji, Phys. Rev. B **79**, 134422 (2009).